IRSTI 29.15.35 https://doi.org/10.26577/RCPh97220267

A.Zh. Zhomartova[1,2], M. Kenessarin[1,2,3,*], K. Nazarov[1,2,3], S.E. Kichanov[2], R.S. Zhumatayev[3], J.-M. Deom[3], A. Smat[3], B. Mukhametuly[1,2,3]
[1]Institute of Nuclear Physics, Almaty, Kazakhstan
[2]Joint Institute for Nuclear Research, Dubna, Russia
[3]Farabi University, Almaty, Kazakhstan
*e-mail: muratkenessarin@inp.kz

MICROSTRUCTURAL AND MINERALOGICAL ANALYSIS OF URYSAY-2 CERAMICS BY X-RAY MICROTOMOGRAPHY AND RAMAN SPECTROSCOPY

The article presents the results of applying X-ray computed tomography (CT) to study the spatial arrangement, size distribution, and morphology of internal inclusions in several ceramic fragments from the Urysay-2 complex in the Zhambyl district of the Almaty region (Republic of Kazakhstan). Based on the tomographic data, segmentation of the internal inclusions was performed, and the grain size of the ancient ceramic samples was calculated. The reconstructions enabled a quantitative morphometric analysis of mineral inclusions, providing statistical distributions of equivalent diameter, elongation, and sphericity. The results revealed significant technological differences: sample C-1 contains the largest and most irregular inclusions (average equivalent diameter ≈ 0.35 mm, mean sphericity ≈ 0.90), whereas C-2 and C-3 show smaller and more uniform grains (average equivalent diameter 0.25–0.30 mm; sphericity up to 0.96), reflecting finer tempering. Raman spectroscopy identified the mineral phases of the samples, including quartz, albite, calcite, hematite, anatase/rutile, and magnetite. The anatase-to-rutile transformation observed in C-2 indicates firing temperatures above ~800 °C under oxidizing conditions. Beyond archaeology, this approach provides a reliable framework for the quantitative characterization of porous ceramics and composite materials in materials science.

Keywords: X-ray microtomography IMAX; Raman spectroscopy; Segmentation; Ancient ceramic microstructure;

А.Ж. Жомартова[1,2], М. Кенесарин[1,2,3,*], Қ. Назаров[1,2,3], С.Е. Кичанов[2], Р.С. Жуматаев[3], Ж.-М. Деом[3], А. Смат[3], Б. Мухаметұлы[1,2,3]
[1]Ядролық физика институты, Алматы, Қазақстан
[2]Біріккен ядролық зерттеу институты, Дубна, Ресей
[3]Әл-фараби атындағы Қазақ ұлттық университеті, Алматы, Қазақстан
*e-mail: muratkenessarin@inp.kz

Рентгендік микротомография және раман спектроскопиясы арқылы Ұрысай 2 керамикасының микроқұрылымдық-минералогиялық талдауы

Мақалада Алматы облысы (Қазақстан Республикасы) Жамбыл ауданындағы «Ұрысай-2» кешенінің бірнеше керамикалық фрагменттеріндегі ішкі қосындылардың кеңістіктік орналасуын, көлемінің таралуын және морфологиясын зерттеу үшін рентгендік компьютерлік томографияны (КТ) қолдану нәтижелері берілген. Томографиялық мәліметтер негізінде ішкі қосындыларды сегменттеу жүргізілді, ежелгі керамикалық үлгілердің түйіршік мөлшері есептелді. Қайта құрулар эквивалентті диаметрдің, ұзарудың және сфераның статистикалық таралуларын қамтамасыз ететін минералды қосындылардың сандық морфометриялық талдауына мүмкіндік берді. Нәтижелер елеулі технологиялық айырмашылықтарды анықтады: С-1 үлгісі ең үлкен және ең дұрыс емес қосындыларды қамтиды (орташа эквивалентті диаметрі ≈ 0,35 мм, орташа сфералық ≈ 0,90), ал С-2 және С-3 кішірек және біркелкі дәндерді көрсетеді (орташа эквиваленттік диаметрі 0,35 мм-ге дейін; 0,96), жақсырақ шыңдауды көрсетеді. Раман спектроскопиясы үлгілердің минералды

фазаларын, соның ішінде кварц, альбит, кальцит, гематит, анатаза/рутил және магнетитті анықтады. С-2-де байқалған анатазаның рутилге айналуы тотықтырғыш жағдайында ~800 °C жоғары күйдіру температурасын көрсетеді. Археологиядан басқа, бұл тәсіл материалтанудағы кеуекті керамика мен композициялық материалдардың сандық сипаттамасының сенімді негізін қамтамасыз етеді.

Түйін сөздер: рентгендік микротомография IMAX, раман спектроскопиясы, сегменттеу, ежелгі керамикалық микроқұрылым.

А.Ж. Жомартова[1,2], М. Кенесарин[1,2,3,*], К. Назаров[1,2,3], С.Е. Кичанов[2],
Р.С. Жуматаев[3], Ж.-М. Деом[3], А. Смат[3], Б. Мухаметулы[1,2,3]
[1]Институт ядерной физики, Алматы, Казахстан
[2]Объединенный институт ядерных исследований, Дубна, Россия
[3]Казахский национальный университет им. аль-Фараби, Алматы, Казахстан
*e-mail: muratkenessarin@inp.kz

Микроструктурный и минералогический анализ керамики Урысай 2 методами рентгеновской микротомографии и рамановской спектроскопии

В статье представлены результаты применения рентгеновской компьютерной томографии (КТ) для изучения пространственного расположения, распределения размеров и морфологии внутренних включений в нескольких фрагментах керамики из комплекса Урысай-2 в Жамбылском районе Алматинской области (Республика Казахстан). На основании томографических данных проведена сегментация внутренних включений и рассчитан размер зерен образцов древней керамики. Реконструкции позволили провести количественный морфометрический анализ минеральных включений, позволив получить статистические распределения эквивалентного диаметра, удлинения и сферичности. Результаты выявили существенные технологические различия: образец С-1 содержит наиболее крупные и нерегулярные включения (средний эквивалентный диаметр ≈ 0,35 мм, средняя сферичность ≈ 0,90), тогда как образец С-2 и С-3 демонстрируют более мелкие и однородные зерна (средний эквивалентный диаметр 0,25–0,30 мм; сферичность до 0,96), что отражает более тонкую закалку. Рамановская спектроскопия позволила идентифицировать минеральные фазы образцов, включая кварц, альбит, кальцит, гематит, анатаз/рутил и магнетит. Наблюдаемое в С-2 превращение анатаза в рутил указывает на температуру обжига выше ~800 °C в окислительных условиях. Помимо археологических исследований, этот подход обеспечивает надежную основу для количественной характеристики пористой керамики и композитных материалов в материаловедении.

Ключевые слова: рентгеновская микротомография IMAX, рамановская спектроскопия, сегментация, древняя керамическая микроструктура.

Introduction

In recent years, the application of non-destructive physical methods has become a leading approach in the study of archaeological artefacts [1,2]. Their ability to preserve unique cultural heritage objects while simultaneously providing quantitative information on structure and composition makes them particularly valuable compared to conventional destructive analyses [3]. Among these techniques, X-ray and neutron methods have proven highly effective for investigating the internal structure of archaeological materials, including weapons [4,5], horse equipment [6], coins [7,8], jewellery [9,10], and ceramics [11–13].

Ceramics, one of the most common categories of archaeological finds, represent a complex multiphase system in which mineral composition, porosity, and inclusion morphology provide direct insights into raw material preparation, firing regimes, and technological traditions of ancient potters [14,15]. Phase composition and microstructural features serve not only as markers of local production practices but also as indicators of cultural exchange and technological innovation [16]. Previous studies [17],

for instance, demonstrated how neutron tomography can classify ceramic fragments from the Byzantine fortress in Dobrudja into distinct technological groups.

X-ray microtomography (micro-CT) has recently emerged as a powerful non-invasive method for visualizing internal heterogeneities with micrometre-scale resolution (10–50 μm). It provides access to morphometric parameters such as equivalent diameter, elongation, and sphericity, enabling statistical descriptions of inclusion and pore populations [18-20]. Complementarily, Raman spectroscopy has proven to be a highly sensitive technique for identifying mineral phases and thermally induced transformations, including the anatase–rutile transition above ~ 800 °C [21] and redox-dependent hematite–magnetite phases [22]. In addition, Raman analysis of carbonaceous phases has been used to estimate firing temperatures of archaeological ceramics from Eastern Kazakhstan [23].

Despite their wide application in European and Asian archaeometry, systematic studies of ceramic complexes from Kazakhstan remain scarce. As part of ongoing research into cultural heritage and the comparative analysis of technological traditions across different regions, the present work applies X-ray microtomography and Raman spectroscopy to ceramic fragments excavated at the Urysay-2 settlement in the Zhambyl district of the Almaty region. The site, first discovered in 2020 by R. Sala and J.-M. Deom, covers an area of 2.5 hectares (100 × 25 m), is naturally sheltered from prevailing winds, and oriented toward southern solar exposure, making it an ideal location for a winter camp [24]. The aim of this study is to apply X-ray microtomography and Raman spectroscopy for the non-destructive characterization of ceramic fragments from Urysay-2, focusing on the quantitative analysis of inclusion morphology and mineralogical composition in order to reconstruct raw material preparation and firing technologies.

Methodology

Description of the Studied Ceramic Materials. The Urysay-2 settlement is located in the upper reaches of the Kyzylkaynar Stream valley (Banditsay, according to local shepherds), 800 meters southwest of the Abdogala farm and stream and 1.8 kilometers south of Mount Karashagyl in the Zhambyl district of the Almaty region (Figure 1). The settlement is located in a gentle gorge between two hills, where surface sherds, possible leveled stepped terraces, and disordered rows of boulders suggest the existence of a settlement with burial objects. Judging by the available sherd types, the settlement was inhabited from the Late Bronze Age (characteristic low-temperature coal-black color with numerous inclusions in the internal composition and red-orange granulated exterior, some with textile imprints), the Early Iron Age, the Medieval Period, and the Ethnographic Period [24]. Four fragments of ceramic pottery were selected for further study (Figure 2).

Raman Spectroscopy. The primary analysis of the phase composition of the ceramic samples was performed using Raman spectroscopy. The experiments were prepared using the LabRam HR spectrometer (Horiba Gr, France) with a Leica M165 microscope equipped with a Ag laser with an excitation wavelength of 633 nm, a x20 objective, an 1800 grating, and a confocal hole of 100 μm. Raman spectra were recorded at different local points on the surface of the studied fragments. All spectra were measured in the range of 50–1800 cm^{-1}, and the exposition for each point was 4-5 min. The tentative identification of the Raman spectra was performed by comparing the obtained spectra with the reference data [25].

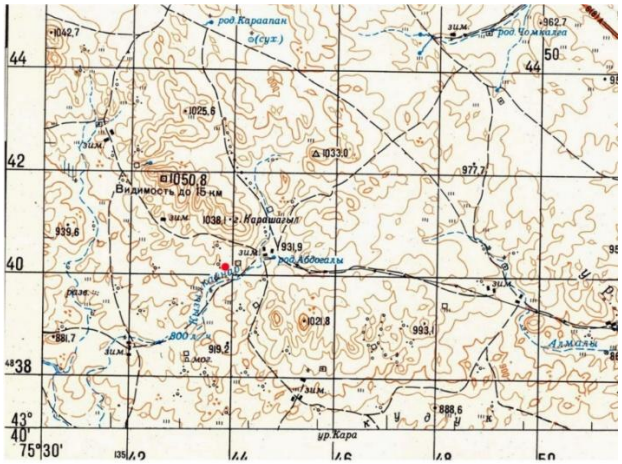

Figure 1 – Topographic map of the settlement Urysay-2 at a scale of 1:100.000 K-43-08

X-ray Microtomography. Tomographic studies were carried out using microtomography to obtain 3D models of the internal structure without destroying the samples. The method is based on the registration of a series of 2D projections during sequential rotation of the sample and subsequent reconstruction of volumetric data using filtered back projection (FBP) in cone geometry. This approach ensures visualization of pores, inclusions and cracks, as well

as quantitative morphometric analysis (volume fraction, size distribution, S/V, etc.) [18]. Measurements were carried out on a specialized IMAX microtomograph (PRODIS Compact), with a Spellman XRB011 microfocus X-ray source [26]. The tomograph operates both in 2D real-time fluoroscopy mode and in 3D tomography mode with a spatial resolution of up to 1 μm. The following parameters were used to study the artifacts: X-ray tube voltage of 70–80 kV, current of 50 μA, image pixel size of 35–45 μm, and voxel size after reconstruction of 35×35 μm2. A 150 μm thick copper filter was used to reduce the low-energy component of the spectrum. Tomographic data were obtained in the step-by-step sample rotation mode: up to 900 projections with an angular step of 0.4°, averaging 5 frames, and an exposure of 100–400 μs. Images were corrected for background noise and normalized by radiation intensity using the ProDIS software package. Image acquisition and adjustment (normalization, adjustment, filtering, and measurements, etc.), and the choice of energies and source current are performed using the ImageJ software package [27], written in Python. Reconstruction and visualization of 3D data were performed using VGStudio MAX 2.2, ImageJ, and its BoneJ module. This method allowed us to obtain detailed 3D models of the studied objects and identify the distribution of inclusions, pores, and cracks.

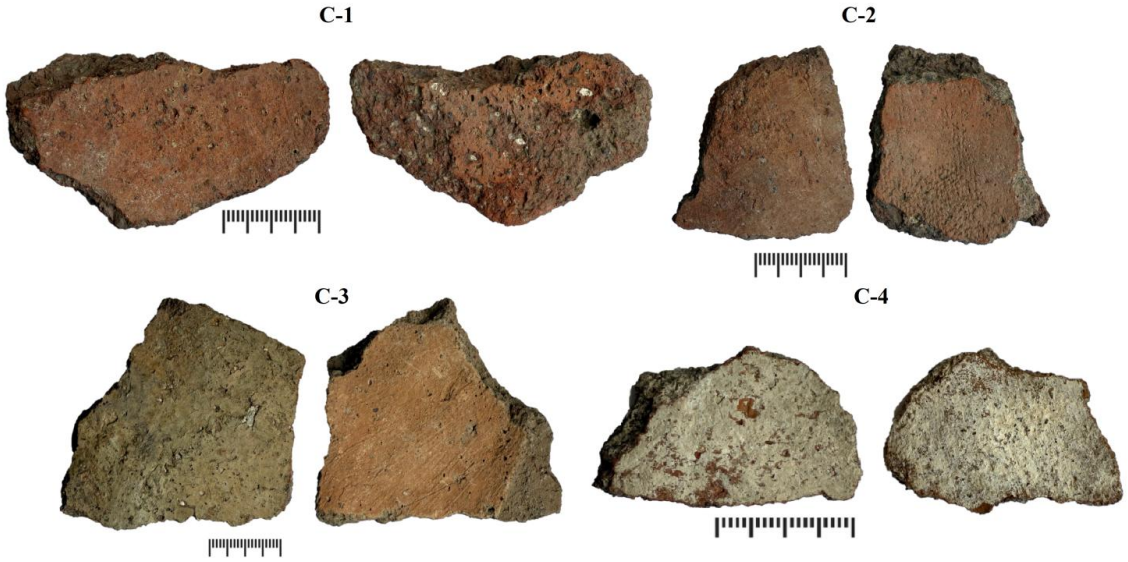

Figure 2 – The photos of the ceramic fragments and its sample labels. The scale bar is shown 2 cm.

Results and discussion

Raman spectroscopy. Using Raman spectroscopy, the mineral composition of ceramic samples from the Urysay-2 site (Almaty region, Kazakhstan). Identified phases include quartz, feldspar (albite), anatase, rutile, carbonaceous matter (D/G bands), calcite, and iron oxides (hematite and magnetite) (Table 1-2). Quartz was detected in all samples with characteristic bands near 127–206–355–464 cm^{-1} [28]. Feldspar was recorded through bands at ~285 and 478–512 cm^{-1}, consistent with albite ($NaAlSi_3O_8$) [29]. Anatase is confirmed by its strong line at ~152 cm^{-1} and accompanying modes at ~396 and 642 cm^{-1}. In sample C-2, rutile was also identified, indicating partial phase transformation of TiO_2 at elevated temperatures in the range of 800–1000 °C [30]. Carbonaceous bands D (~1330–1346 cm^{-1}) and G (~1560–1575 cm^{-1}) were present in all samples, suggesting organic temper or incomplete combustion during firing [23]. Calcite (ν1 ~1087–1088 cm^{-1}) was found in C-1 and C-3, while hematite (Fe_2O_3) and magnetite (Fe_3O_4) were variably present [31]. In sample C-1, the coexistence of calcite and hematite suggests either moderate firing temperatures (≤750–800 °C) in an oxidizing atmosphere or secondary recrystallization of calcite within pores after firing. The presence of rutile in C-2 reflects the anatase → rutile transition, which occurs at temperatures above ~800 °C [30, 32]. Together with hematite, this indicates the highest-temperature oxidizing conditions among all samples. In contrast, samples C-1 and C-3 with calcite and anatase reflect moderate firing temperatures, whereas C-4 likely experienced higher temperatures under reducing conditions. Redox atmosphere: hematite in C-1–C-3

points to predominantly oxidizing conditions, while magnetite in C-4 indicates a reducing atmosphere [33]. The dominance of magnetite together with carbon bands suggests reducing or fluctuating redox conditions with incomplete combustion of organic matter.

Table 1 – Representative samples with mineralogical composition and the list of Raman band position characteristic of the various compounds (w–weak, m–medium, s–strong).

Sample	Mineral phases	Main vibrational bands (cm^{-1})
C-1	Quartz (SiO_2)	123(m), 202(m), 355(w), **463(s)**
	Calcite ($CaCO_3$)	**1088(s)**
	Albite $Na(AlSi_3O_3)$	160(m), 285(m), 408(w), **478**(s), **506**(s)
	Carbon	**1334**(s), **1560**(s)
	Hematite (Fe_2O_3)	**184**(s), **250**(s), 406(m), 462(m), 688(m)
C-2	Quartz (SiO_2)	128(m), 204(m), **465**(s)
	Anatase (TiO_2)	**152**(s), 205(w), 396(w), 510(w), 642(m)
	Carbon	**1334**(s), **1573**(s)
	Albite $Na(AlSi_3O_3)$	156(m), 285(m), 401(w), 462(m), 511(m)
	Hematite (Fe_2O_3)	**216**(s), **277**(s), 463(w), 1307(w)
	Rutile (TiO_2)	143(w), 232(m), 415(s), 606(s)
C-3	Quartz (SiO_2)	124(m), 195(m), 352(w), **462**(s)
	Anatase (TiO_2)	**152**(s), 203(w), 394(w), 508(w), 632(m)
	Calcite ($CaCO_3$)	**1087**(s)
	Carbon	**1344**(s), **1565**(s)
	Albite $Na(AlSi_3O_3)$	158(m), 286(m), 407(w), **477**(s), **512**(s)
	Hematite (Fe2O3)	**212**(s), **277**(s)
C-4	Quartz (SiO_2)	127(m), 206(m), 351(w), **464**(s)
	Anatase (TiO_2)	**151**(s), 205(w), 403(w), 510(w), 633(m)
	Carbon	**1346**(s), **1575**(s)
	Magnetite (Fe_3O_4)	206(m), 299(m), 473(s), **670**(s)

Table 2 – Distribution of mineral phases in ceramic samples based on Raman spectroscopy results. The "+" sign indicates positive phase identification

Sample	Observed phases						
	Quartz	Anatase	Albite	Carbon	Calcite	Hematite	Magnetite
C-1	+		+	+	+	+	
C-2	+	+	+	+		+	
C-3	+	+	+	+	+	+	
C-4	+	+		+			+

X-Ray Microtomography. Three-dimensional 3D models of ceramic fragments (C-1–C-4) from the Urysay-2 complex were obtained using X-ray computed tomography (Figure 3). The distribution of internal heterogeneities, inclusion sizes (Table 3, Supplementary materials), pores, and cracks in the samples were taken from these models. Virtual sections (Figure 3 (b,d)) reflected the internal component distributions and density differences. The X-ray interaction intensity, varying from blue (low) to red (high), indicated compositional differences. The reconstructed 3D models of the samples (Figure 3) revealed significant differences in their internal structure. Sample C-4 exhibits a high inclusion

content of ~1.15% of the total volume (Table 3). In contrast, sample C-3 has a more uniform structure and the lowest inclusion rate (~0.12%), indicating a dense composition and uniform firing. The radiographic image also reveals numerous pores and cracks that formed during the firing of the ceramic ware.

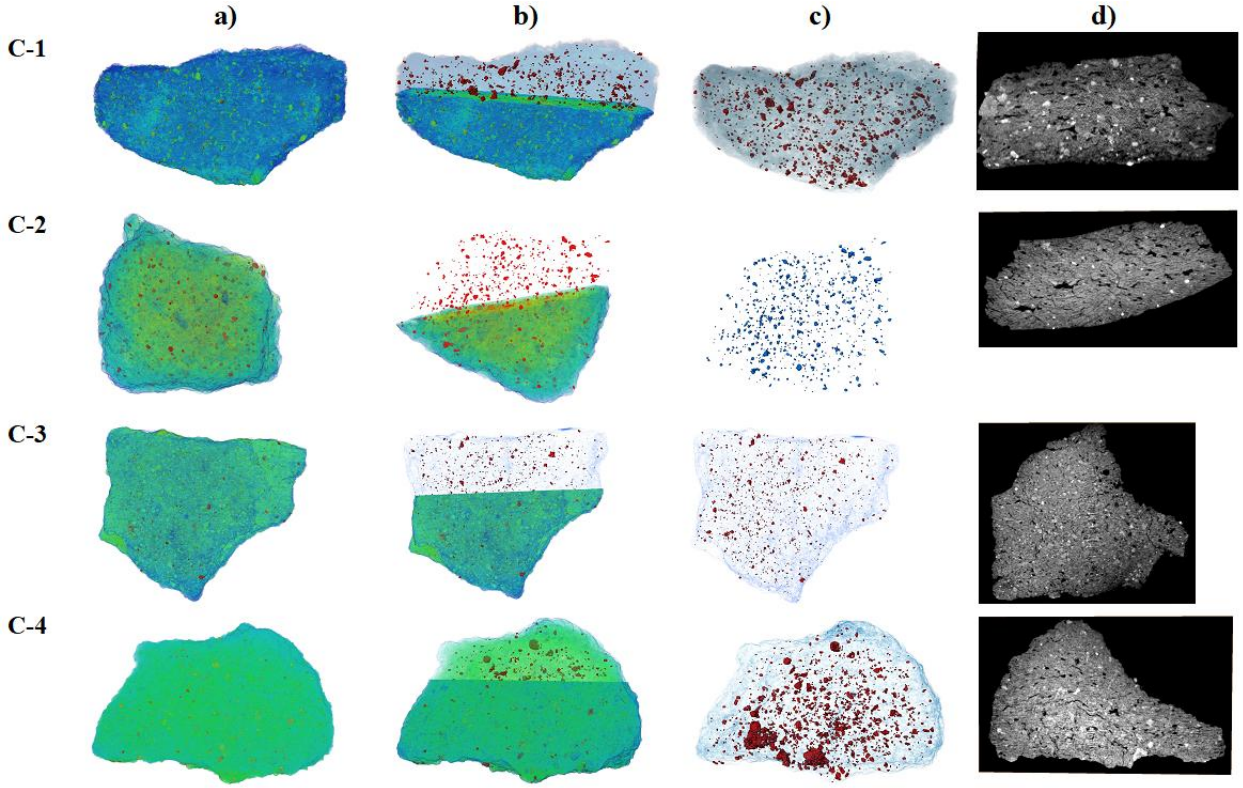

Figure 3 – 3D models (a) created after tomographic reconstruction and selected longitudinal sections (c) of a ceramic fragment. Rainbow coloring shows the degree of X-ray absorption from low (blue) to high (red). Internal features and inclusions are highlighted in green-red (b).

Table 3 – Calculated data on the volume of components of the studied ceramic fragments from computed tomography analysis.

Sample	Total Volume, voxel	Impurities Volume, voxel	Proportion of Impurities, %
C-1	311598784	1703699	0.55(1)
C-2	249769808	540539	0.25
C-3	617243008	743420	0.12
C-4	94542632	1088434	1.15

After segmenting the inclusions from the volume of the studied ceramic fragments, the sizes of these internal inclusions were studied and the equivalent diameter, elongation, and sphericity were quantified (Figure. 4–5, Supplementary Materials). The equivalent diameter parameter was used to estimate pore sizes [34].

$$D = \sqrt[3]{6 \times V/\pi}, \quad (1)$$

D – EqDiameter; V – volume 3D; π – pi number;

The average inclusion size varies from 0.25 to 0.35 mm, with median values between 0.21 and 0.30 mm. C-1 contains the largest inclusions on average (mean ≈ 0.35 mm, median ≈ 0.30 mm), while C-2 and C-3 are characterized by smaller and more uniform grains (mean ≈ 0.25–0.30 mm, median ≈ 0.21–0.25 mm). C-4 exhibits the widest size distribution, ranging from 0.13 mm up to 2.67 mm, consistent with less purified raw material. The statistical distribution of inclusion sizes appeared complex and multimodal. To analyse it, we employed non-parametric kernel density estimation of the probability density function,

with the optimal bandwidth determined by Silverman's criterion [35]. In this approach, we can compare the calculated distributions from one sample to another.

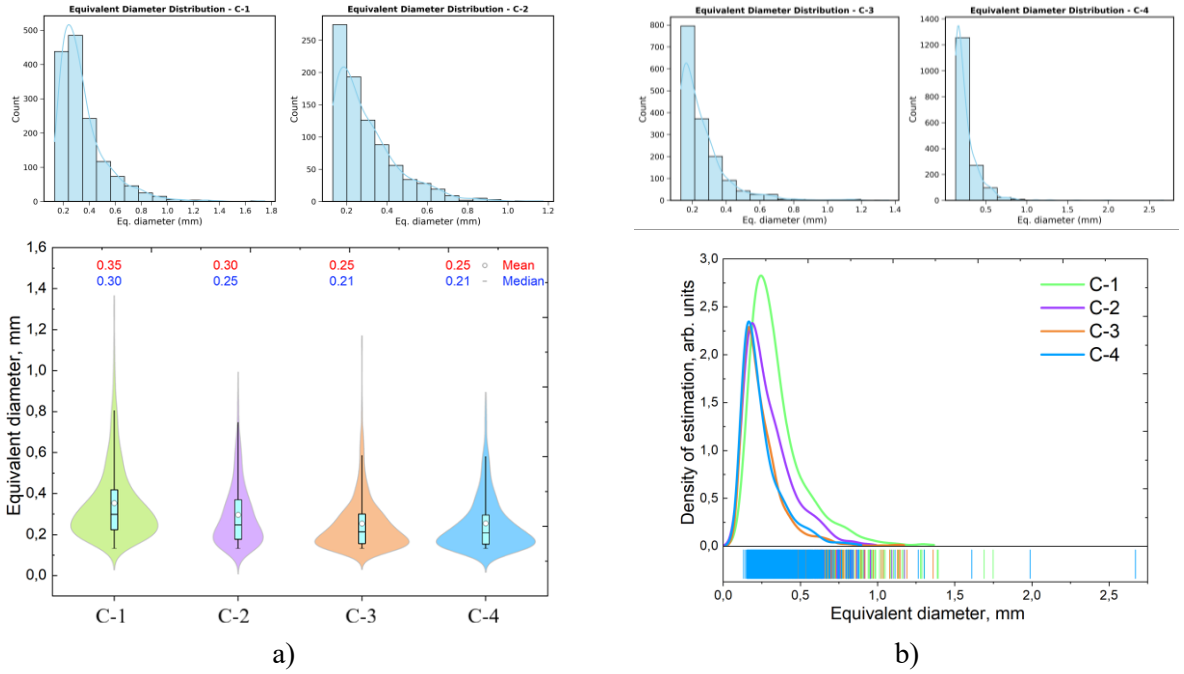

a) b)

Figure 4 – (a) Violin plot of the distribution of data and the probability density of equivalent inclusion diameter. Calculated values of average and median inclusion sizes are presented at top. (b) Probability density function of equivalent diameter distribution is shown on the right.

The violin plots of equivalent diameter (Figure 4a) demonstrate distinct distribution patterns. Samples C-3 and C-4 display bimodal distributions, with populations of both fine and coarse inclusions. C-1 shows an asymmetric distribution with a long tail towards larger sizes, while C-2 is characterized by a narrow, nearly unimodal distribution, reflecting careful clay preparation. Kernel density estimation further highlights these differences, with well-defined maxima in C-3 and C-4. The next parameter that further differentiates the samples is the elongation of the internal inclusions ($E = 1 - b/a$, where a and b are the main axes of the ellipse/ellipsoid) [36]. Elongation values cluster around 0.6–0.7 for most samples, indicating predominantly sub-isometric shapes, though larger inclusions tend to be more elongated. Probability density functions of elongation (Figure 5a) exhibit two maxima: one near ~0.5 (flattened particles, aspect ratio ~1:2) and another near ~1.0 (isometric forms). This suggests a mixture of rounded temper grains and elongated fragments. Correlation analysis confirms a positive relationship between inclusion size and elongation ($r \approx 0.47$; Figure 5b), meaning that larger inclusions are generally more anisometric. Also, with tomography, we determined the sphericity of inclusions

$$\Psi = \frac{\pi^{1/3} \times (6 \times V)^{2/3}}{S},$$

Ψ – sphericity; π – pi number; V – Volume 3D; S – Area 3D; which made it possible to obtain additional information about the studied samples (Supplementary materials).

Sphericity values support these observations. C-2 and C-3 have the most rounded inclusions (mean $\Psi \approx 0.96$–0.97), consistent with refined temper and stable firing conditions. C-1 shows slightly lower sphericity (mean $\Psi \approx 0.90$), reflecting the presence of irregular particles. C-4 exhibits the lowest values (mean $\Psi \approx 0.94$), together with a wide range (0.23–1.0), indicating the use of coarser, angular fragments.

Overall, X-ray tomography reveals a technological contrast: C-2 and C-3 represent carefully prepared ceramics with uniform microstructures, while C-1 and especially C-4 reflect the use of heterogeneous raw materials and coarser tempering practices. These differences are consistent with the coexistence of parallel production traditions within the Urysay-2 settlement.

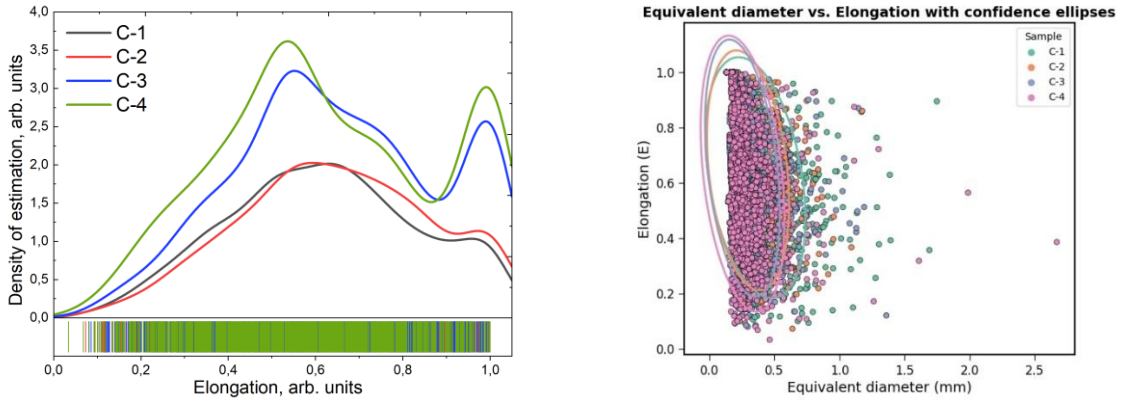

a) b)

Figure 5 – (a) Probability density function of the elongation (b) distribution of inclusions in ceramic fragments.

Conclusions

This study demonstrates the effectiveness of combining X-ray microtomography and Raman spectroscopy for the non-destructive characterization of ancient ceramics from Kazakhstan. Raman spectroscopy identified quartz, feldspar, calcite, hematite, anatase/rutile, and magnetite as mineralogical markers of firing temperature and redox conditions. X-ray microtomography provided quantitative morphometric parameters of inclusions, revealing significant technological variability between the samples. This work demonstrates the potential of non-destructive physical methods for the quantitative characterization of ancient ceramics and highlights their broader applicability to the study of porous and composite materials.

Acknowledgments

This work was supported by the Committee of Science of the Ministry of Science and Higher Education of the Republic of Kazakhstan under Grant No. AP23490652.

Author Contributions

A.Zh. Zhomartova: Conceptualization, Methodology, Writing – original draft; **M. Kenessarin:** Investigation, Data curation, Resources; **K. Nazarov:** Conceptualization, Investigation, Data curation, Resources; **S.E. Kichanov:** Supervision, Conceptualization, Writing – review & editing; **R.S. Zhumatayev:** Methodology, Investigation; **J.-M. Deom:** Investigation, Data curation; **A. Smat**: Investigation, Writing – review & editing; **B. Mukhametuly:** Project administration, Investigation, Methodology.

References

1. P. Singh, E. Mal, A. Khare, and S. Sharma, A study of archaeological pottery of Northeast India using laser induced breakdown spectroscopy (LIBS), *J. Cult. Herit.* **33**, 71-82 (2018). https://doi.org/10.1016/j.culher.2018.03.011

2. M. Mednikova, I. Saprykina, S. Kichanov, and D. Kozlenko, The Reconstruction of a Bronze Battle Axe and Comparison of Inflicted Damage Injuries Using Neutron Tomography, Manufacturing Modeling, and X-ray Microtomography Data, *J. Imaging* 6, 45 (2020). https://doi.org/10.3390/jimaging6060045

3. N. Kardjilov, F. Fiori, G. Giunta, A. Hilger, F. Rusticheli, M. Strobl, J. Banhart, and R. Triolo, Neutron tomography for archaeological investigations, *J. Neutron. Res.* 14, 29–36 (2006). https://doi.org/10.1080/10238160600673201

4. A. Fedrigo, M. Strobl, A.R. Williams, K. Lefmann, P.E. Lindelof, L. Jørgensen, P. Pentz, D. Bausenwein, B. Schillinger, and A. Kovyakh, Neutron imaging study of 'pattern-welded' swords from the Viking Age, *Archaeol. Anthropol. Sci.* 10, 1249–1263 (2018). https://doi.org/10.1007/s12520-016-0454-5

5. F. Grazzi, F. Cantini, F. Salvemini, A. Scherillo, B. Schillinger, A. Kaestner, D. Edge, and A. Williams, The investigation of Indian and central Asian swords through neutron methods, *J. Archaeol. Sci. Rep.* 20, 834–842, (2018). https://doi.org/10.1016/j.jasrep.2018.06.010

6. A. Zh. Zhomartova, K. M. Nazarov, M. Kenessarin, Z. S. Samashev, R. S. Zhumatayev, D. M. Janseitov, and S. E. Kichanov, The neutron imaging studies of the metal archaeological objects from the Eleke Sazy complex, *Eurasian J. Phys. Funct. Mater.* 8, 79-83, (2024). https://doi.org/10.69912/2616-8537.1189

7. B. Bakirov, I. Saprykina, S. Kichanov, R. Mimokhod, N. Sudarev, and D. Kozlenko, Phase Composition and Its Spatial Distribution in Antique Copper Coins: Neutron Tomography and Diffraction Studies, *J. Imaging* 7, 129 (2021).

https://doi.org/10.3390/jimaging7080129

8. F. Salvemini, S. R. Olsen, V. Luzin, U. Garbe, J. Davis, T. Knowles, and K. Sheedy, Neutron tomographic analysis: Material characterization of silver and electrum coins from the 6th and 5th centuries BCE, *Mater. Charact.* **118**, 175–185, (2016). https://doi.org/10.1016/j.matchar.2016.05.018

9. N. Kardjilov, and F. Giulia (2017), *Neutron Methods for Archaeology and Cultural Heritage*. Springer.

10. I.A. Saprykina, E.A. Khairedinova, S.E. Kichanov, A. V. Rutkauskas, N. M. Belozerova, and D. P. Kozlenko, *Archaeol. Cult. Anthropol.* **4**, 167–181 (2022). https://doi.org/10.55086/sp224167181

11. B.A. Abdurakhimov, S.E. Kichanov, C. Talmatchi, D.P. Kozlenko, G. Talmatchi, N. M. Belozerova, M. Balasoiu, and M. C. Belc, Studies of ancient pottery fragments from Dobrudja region of Romania using neutron diffraction, tomography and Raman spectroscopy, *J. Archaeol. Sci Rep.* **35**, 102755 (2021). https://doi.org/10.1016/j.jasrep.2020.102755

12. A.Zh. Zhomartova, B.A. Bakirov, S.E. Kichanov, R.S. Zhumatayev, A.T. Toleubayev, S. Shakenov, and D. P. Kozlenko, Non-destructive structural studies of ceramic fragments of ancient tribes of Kazakhstan, *Eurasian J. Phys. Funct. Mater*. **7**, 79-90 (2023). https://doi.org/10.32523/ejpfm.2023070201

13. M. Kenessarin, K. Nazarov, V. Smirnova, S. Kichanov, N.Torezhanova, O. Myakisheva, A. Zhomartova, B. Mukhametuly, R. Nemkayeva, and E. Myrzabekova, An Analysis of the Pore Distribution in Ceramic Vessels from the Akterek Burial Archeological Site Using Neutron Tomography Data, *Heritage* **8**, 210, (2025). https://doi.org/10.3390/heritage8060210

14. M.S. Tite, Ceramic production, provenance and use - a review, *Archaeometry* **50**, 216–231 (2008). https://doi.org/10.1111/j.1475-4754.2008.00391.x

15. G. Eramo, A. Mangone, Archaeometry of ceramic materials, *Phys. Sci. Rev.* **4**, *(*2019). https://doi.org/10.1515/psr-2018-0014

16. S. Huang, B. Xue, Y. Zhao, and J. Yang, Characterization of primary silicate minerals in Earth-like bodies via Raman spectroscopy, *J. Raman Spectrosc.* **55**, 625–636 (2024). https://doi.org/10.1002/jrs.6657

17. A.Z. Zhomartova, B.A. Abdurakhimov, C. Talmațchi, S.E. Kichanov, D.P. Kozlenko, M. Bălășoiu, G. Talmațchi, C. Șova, and M.C. Belc, The systematic structural studies of some Byzantine ceramic fragments from Dobrudja region of Romania: Raman spectroscopy, neutron diffraction, and imaging data, *Archaeometry* **66**, 787–802 (2024). https://doi.org/10.1111/arcm.12947

18. Z. Lin, Y. Deng, L. He, Z. Peng, and X. Duan, Microscale Investigation of Aggregate Stability Characteristic and Pore Structure of Collapsing Wall in Granite Red Soil, *Land Degrad. Dev*. 1–16 (2025). https://doi.org/10.1002/ldr.70106

19. D. Braun, *Am Antiq* **47**, 55–71 (1982).

20. P.R. Thomson, R. Ellis, D. Chiarella, and S. Hier-Majumder, Microstructural Analysis From X-Ray CT Images of the Brae Formation Sandstone, North Se, *Front. Earth Sci.* **8**, 246 (2020). https://doi.org/10.3389/feart.2020.00246

21. P. McManus, and S. Fleming, *J. Mater. Sci.* **31**, 4567–4573 (1996).

22. D.L.A. de Faria, and F. N. Lopes, *J. Raman Spectrosc.* **28**,873–878 (2007).

23. B. Bakirov, A. Zhomartova, S. E. Kichanov, R. Zhumatayev, A. T. Toleubayev, K. Nazarov, D. Kozlenko, and A. M. Nazarova, Non-destructive neutron structural studies of ancient ceramic fragments of the cultural heritage of the Republic of Kazakhstan, *Eur. J. Phys. Funct. Mater.* **6**, 56–70 (2022). https://doi.org/10.32523/ejpfm.2022060106

24. R. Sala, and J.-M.Deome, Cultural landscape of Mount Karashagyl in the south-eastern part of the Chu-Ili Mountains // "XV Orazbaev oculary" halykaralyk gylymi-adistemelik conferensia materialdary / ed. R.S. Zhumataev. – Almaty: Kazakh University, 2023. P.108-113. (in Russ.)

25. B. Lafuente, R.T. Downs, H. Yang, and N. Stone, The power of databases: The RRUFF project, *Highlights Miner. Crystallogr.*1–30 (2015). https://doi.org/10.1515/9783110417104-003

26. I. Chuprakov, K. Nazarov, B. Mukhametuly, A. Bekbayev, Y. Arynbek, M. Kenessarin, Y. Bazarbayev, E. Myrzabekova, A. Nazarova, B. Abdurakhimov, and I. Zel, IMAX – a compact x-ray microtomography instrument for material research, *Herald Kazakh-Brit. Tech. Univ.* **22**, 298-306 (2025). https://doi.org/10.55452/1998-6688-2025-22-1-298-306

27. C.A. Schneider, W.S. Rasband, and K.W. Eliceiri, NIH Image to ImageJ: 25 years of image analysis, *Nat. Methods* **9**, 671–675 (2012). https://doi.org/10.1038/nmeth.2089

28. N. Buzgar, A. I. Apopei, and A. Buzatu, Characterization and source of Cucuteni black pigment (Romania): vibrational spectrometry and XRD study, *J. Archaeol. Sci.* **40**, 2128–2135 (2013). https://doi.org/10.1016/j.jas.2012.12.034

29. J.J. Freeman, A. Wang, K.E. Kuebler, B.L. Jolliff, and L.A. Haskin, Characterization of natural feldspars by raman spectroscopy for future planetary exploration, *Can. Mineral.* **46**, 1477–1500 (2008). https://doi.org/10.3749/canmin.46.6.1477

30. O. Boytsova, I. Zhukova, A. Tatarenko, T. Shatalova, A. Beiltiukov, A. Eliseev, and A. Sadovnikov, The Anatase-to-Rutile Phase Transition in Highly Oriented Nanoparticles Array of Titania with Photocatalytic Response Changes, *Nanomaterials* **12**, 4418 (2022). https://doi.org/10.3390/nano12244418

31. L. Medeghini, P.P. Lottici, C. De Vito, S. Mignardi, and D. Bersani, Micro-Raman spectroscopy and ancient ceramics: applications and problems, *J. Raman Spectrosc.* **45**, 1244–1250 (2014). https://doi.org/10.1002/jrs.4583

32. D.A. H. Hanaor, and C.C. Sorrell, Review of the anatase to rutile phase transformation, *J. Mater. Sci.* **46**, 855–

874 (2011). https://doi.org/10.1007/s10853-010-5113-0

33. K.F. McCarty, M. Monti, S. Nie, D.A. Siegel, E. Starodub, F.E. Gabaly, and J.D.L. Figuera, Oxidation of Magnetite(100) to Hematite Observed by in Situ Spectroscopy and Microscopy, *J. Phys. Chem. C* **118**, 19768-19777 (2014). https://doi.org/10.1021/jp5037603

34. I.Y. Zel, M. Kenessarin, S.E. Kichanov, M. Balasoiu, D.P. Kozlenko, K. Nazarov, M. Nicu, L. Ionascu, A.C. Dragolici, and F. Dragolici, Spatial distribution of graphite in cement materials used for radioactive waste conditioning: An approach to analysis of neutron tomography data, *Cem. Concr. Compos.* **119**, 103993 (2021). https://doi.org/10.1016/j.cemconcomp.2021.103993

35. J.S. Simon, Density Estimation, *Statist. Sci.* **19** 588 – 597 (2004). https://doi.org/10.1214/088342304000000297

36. V. Angelidakis, S. Nadimi, and S. Utili, Elongation, flatness and compactness indices to characterise particle form, *Powder Technol*. **396**, 689–695 (2022). https://doi.org/10.1016/j.powtec.2021.11.027

Information about authors:

Ayazhan Zhomartova – Senior Researcher, Laboratory of Neutron Physics, Institute of Nuclear Physics, (Almaty, Kazakhstan; e-mail: zhomartova@jinr.ru).

Murat Kenessarin (corresponding author) – Junior researcher, Laboratory of Neutron Physics, Institute of Nuclear Physics, (Almaty, Kazakhstan, e-mail: muratkenessarin@inp.kz).

Kuanysh Nazarov – Head of laboratory, Laboratory of neutron physics, Institute of Nuclear Physics, (Almaty, Kazakhstan; e-mail: k.nazarov@inp.kz).

Sergey Kichanov – Head of the DN-12 group, Frank Laboratory of Neutron Physics, Joint Institute of Nuclear Research, (Dubna, Russia; e-mail: ekich@nf.jinr.ru).

Rinat Zhumatayev – Head of the department of archaeology, ethnology and museology, faculty of history, Al-Farabi Kazakh National University, (Almaty, Kazakhstan; e-mail: zhumatayevr@gmail.com).

Jean-Marc Deom, Researcher, faculty of history, Al-Farabi Kazakh National University, (Almaty, Kazakhstan; e-mail: jeandeom@kaznu.kz).

Aiaru Smat – Master's student, faculty of physics and technology, Al-Farabi Kazakh National University, (Almaty, Kazakhstan; e-mail: aiarualtaikhan01@gmail.com).

Bagdaulet Mukhametuly – Senior Researcher, Laboratory of Neutron Physics, Institute of Nuclear Physics, (Almaty, Kazakhstan; e-mail: bagdaulet_m@inp.kz).

Авторлар туралы мәлімет:

Аяжан Жомартова – аға ғылыми қызметкер, нейтрондық физика зертханасы, ядролық физика институты, (Алматы, Қазақстан; e-mail: zhomartova@jinr.ru).

Мұрат Кенесарин (автор-корреспондент) – кіші ғылыми қызметкер, нейтрондық физика зертханасы, ядролық физика институты, (Алматы, Қазақстан; e-mail: muratkenessarin@inp.kz).

Қуаныш Назаров – зертхана меңгерушісі, нейтрондық физика зертханасы, ядролық физика институты, (Алматы, Қазақстан; e-mail: k.nazarov@inp.kz).

Сергей Кичанов – НД-12 тобының басшысы, Франк нейтрондық физика зертаханасы, Біріккен ядролық зерттеу институты, (Дубна, Ресей; e-mail: ekich@nf.jinr.ru).

Ринат Жуматаев – археология, этнология және мұражайтану кафедрасының меңгерішсі, тарих факультеті, Әл-фараби ат. Қазақ ұлттық университеті, (Алматы, Қазақстан; e-mail: zhumatayevr@gmail.com).

Жан-Марк Деом – зерттеуші, тарих факультеті, Әл-Фараби атыңдағы Қазақ ұлттық университеті, (Алматы, Қазақстан; e-mail: jeandeom@kaznu.kz).

Айару Смат – магистрант, физика техникалық факультеті, Әл-Фараби атыңдағы Қазақ ұлттық университеті, (Алматы, Қазақстан; e-mail: aiarualtaikhan01@gmail.com).

Бағдәулет Мұхаметұлы – аға ғылыми қызметкер, нейтрондық физика зертханасы, Ядролық физика институты, (Алматы, Қазақстан; e-mail: bagdaulet_m@inp.kz).

Сведения об авторах:

Аяжан Жомартова – старший научный сотрудник, лаборатория нейтронной физики, Институт ядерной физики (Алматы, Казахстан; e-mail: zhomartova@jinr.ru).

Мурат Кенессарин (автор-корреспондент) – младший научный сотрудник, Лаборатория нейтронной физики, Институт ядерной физики (Алматы, Казахстан; e-mail: muratkenessarin@inp.kz).

Куаныш Назаров – заведующий лабораторией, Лаборатория нейтронной физики, Институт ядерной физики (Алматы, Казахстан; e-mail: k.nazarov@inp.kz).

Сергей Кичанов – руководитель группы ДН-12, Франковская лаборатория нейтронной физики, Объединенный институт ядерных исследований (Дубна, Россия; e-mail: ekich@nf.jinr.ru).

Ринат Жуматаев – заведующий кафедрой археологии, этнологии и музеологии исторического факультета Казахского национального университета им. аль-Фараби (Алматы, Казахстан; e-mail: zhumatayevr@gmail.com).

Деом Жан-Марк – научный сотрудник исторического факультета Казахского национального университета им. аль-Фараби (Алматы, Казахстан; e-mail: jeandeom@kaznu.kz).

Айару Смат – магистрант физико-технического факультета Казахского национального университета им. аль-Фараби (Алматы, Казахстан; e-mail: aiarualtaikhan01@gmail.com).

Багдолет Мухаметули – старший научный сотрудник лаборатории нейтронной физики Института ядерной физики (Алматы, Казахстан; e-mail: bagdaulet_m@inp.kz).

Article history: *received: 16 February 2026; revised: 01 April; accepted: 18 May 2026.*
Мақала тарихы*: түсті: 16 ақпан 2026; түзетілді: 01 сәуір; қабылданды: 18 мамыр 2026.*
История статьи: *поступила: 16 февраля 2026; после доработки 01 апреля; принята: 18 мая 2026.*